Check for updates

Orientational control of quantum interference in ferrocene single-molecule junctions

Karimah Alresheedi,†[ab] Asma Alajmi,†[ac] Adel Alrehaili,[ad] Alaa Al-Jobory, [ID][ae] Colin Lambert [ID] *[a] and Ali Ismael [ID] *[af]

In single-molecule junctions, quantum interference (QI) effects manifest even at room temperature and can be explained by simple quantum circuit rules (QCR), and a rather intuitive magic ratio (MR), theory. These rules characterise how individual moieties contribute to the overall electrical conductance (G), of a molecule and how the overall G can change when the connectivities between different moieties is varied. Here we examine the electrical conductance of a single-ferrocene junction when the two metal electrodes connect to both upper and lower cyclopentadienyl (CP) rings and compare this with the conductance when both electrodes are contacted to only the upper CP ring. In the case of the former, the angle of rotation θ between the upper and lower rings could be changed by varying the distance between the electrodes. The main aim of our investigation is to determine how QI within the ferrocene core is affected by the length of linker groups, which connect the core to electrodes. We find that when $\theta = 0$, short and long molecules exhibit destructive QI (DQI) features within the HOMO−LUMO gap, whereas as θ is increased, the DQI is alleviated. However, DQI within the HOMO−LUMO gap is alleviated at entirely different rotation angles of $\theta > 20°$ for the molecule with longer linkers, compared to $>60°$ for the shorter molecule. This shows that interference patterns within the ferrocene core are not simply a property of the core alone, but are a holistic property of the molecule as a whole. We investigated the Seebeck coefficients S of these molecules and found that S of the longer molecules can reach 250 μV K^{-1}, which is significantly higher that the Seebeck coefficients of the shorter molecules.

1. Introduction

Ferrocene is an organometallic compound with a unique ''*sandwich*'' structure,[1–5] where an iron atom is coordinated between two cyclopentadienyl (C_5H_5) rings. Ferrocene is known for its high stability in aqueous and aerobic media.[6–8] Since its discovery in 1951,[9,10] ferrocene has attracted considerable interest in molecular electronics, because of its distinctive electrical properties and potential quantum interference effects in molecular junctions.[11–15] Quantum interference (QI), in molecular junctions is a significant phenomenon that can either boost or inhibit electron movement based on the

molecule arrangement and electronic structure.[16–19] Some studies illustrated that branched molecular junctions, especially those containing ferrocene, display both constructive quantum interference (CQI) and destructive quantum interference (DQI) effects. CQI can arise from symmetrically equivalent pathways through the molecular branches, there facilitating electrical conductance in some cases. On the other hand, DQI significantly reduces electron transport, especially in *meta*-connected systems.[20–24] Several articles have investigated the mechanical tunability of quantum interference in ferrocene-based single-molecule junctions.[25–32] For instance, Camarasa-Gómez *et al.*[1] recently demonstrated that the conductance of ferrocene derivatives could be substantially adjusted by modifying the junction configuration, with DQI resulting from the hybridisation of metal-based d-orbitals and the ligand-based π-system. This mechanical regulation of quantum interference underscores the potential for creating molecular devices with customised electrical characteristics.

The integration of ferrocene into molecular wires has demonstrated an increase in conductance by diminishing the tunnelling barrier and aligning molecular orbitals with the metal Fermi level. Lu *et al.*[33] found that the electronic structure, specifically the energy gap between the highest occupied

a Physics Department, Lancaster University, Lancaster, LA1 4YB, UK

b Department of Physics, College of Science, Qassim University, Buraydah 51402, Saudi Arabia. E-mail: c.lambert@lancaster.ac.uk, k.ismael@lancaster.ac.uk

c Department of Physics, College of Science and Humanities in Al-Kharj, Prince Sattam Bin Abdulaziz University, Al-Kharj 11942, Saudi Arabia

d Physics Department, Faculty of Science, Islamic University of Madinah, Madinah, 42351, Saudi Arabia

e Department of Physics, College of Science, University of Anbar, Anbar, Iraq

f Department of Physics, College of Education for Pure Science, Tikrit University, Tikrit, Iraq

† These authors contributed equally to this work.

molecular orbital (HOMO) and the lowest unoccupied molecular orbital (LUMO), is essential in influencing the charge transport characteristics of ferrocene-containing systems. This corresponds with the findings of Sun *et al.*[34] who observed that the incorporation of ferrocene into alkanes markedly enhanced electron transport, which they ascribed to the advantageous electronic interactions enabled by the ferrocene moiety. These and related studies demonstrate that ferrocene's stable redox behaviour, conformational flexibility, and ability to facilitate electron transfer make it a key component in charge transport, catalytic processes, and energy storage applications.[35–43] Theoretical investigations have clarified the spin-dependent transport characteristics of ferrocene-based junctions.[44–47] For example, Yuan *et al.*[44] examined the spin-filtering efficiency in ethynyl-terminated ferrocene junctions, demonstrating that the position of terminal group substitutions significantly influences the spin-dependent current–voltage characteristics. Their findings indicate that modifying the molecular configuration alters spin polarisation and electronic transport, highlighting ferrocene's potential for spintronic applications. Their study also suggests that quantum interference can be exploited to control spin states, providing a foundation for designing spin-based molecular devices such as spin transistors and molecular spin filters.

Here we investigate the quantum transport properties of four ferrocene-based derivatives by analysing their transmission coefficients to determine whether the quantum interference is constructive or destructive. Using a combination of computational quantum transport simulations and theoretical models, we explore the role of molecular geometry, electronic interactions, and substituent effects in electron transport. These structures consist of a ferrocene unit, with two thioanisole gold-binding groups, linked to either on the same or opposite cyclopentadienyl (Cp), rings.[1] In particular, we investigate how QI through the ferrocene core is changed when the length of the linkers is changed from the short linkers of **1** and **2**, to the longer linkers of **3** and **4**, as shown in Fig. 1 below. It should be noted that our molecules (**3** and **4**) differ from those studied in ref. 1 (**1** and **2**) in molecular length. Specifically, compounds **3** and **4** incorporate two additional triple bonds

(–C≡C–), extending their length by approximately 5 Å compared to **1** and **2**.

2. Methods

To calculate electron transport through the ferrocene core, we began by modelling the terminal SMe-Au binding energetics and then relaxed each compound in the presence of fixed electrodes. Using the density functional code SIESTA[48] (for more detail, see the geometry of isolated ferrocene in the SI), the optimum geometries of isolated ferrocene derivatives were obtained by relaxing the molecules until all forces on the atoms were less than 0.01 eV Å^{-1} (see Fig. S2). We used a double-zeta plus polarization orbital basis set, norm-conserving pseudopotentials, the local density approximation (LDA) exchange–correlation functional, and to define the real space grid, an energy cutoff of 250 Rydbergs. We also computed results using GGA and found that the resulting transmission functions were comparable[49,50] with those obtained using LDA. To simulate the likely contact configuration during a break-junction experiment, we employed electrodes constructed from 5 layers of Au (111), each containing 30 gold atoms and further terminated with a pyramid of gold atoms. After relaxing each molecular junction in different orientations, we calculated the electrical conductance using the Gollum quantum transport code,[18] (for more details see Section 5 of the SI).

3. Results and discussion

The optimal binding distance between the electrodes and the thiomethyl anchor groups were obtained by calculating their binding energies as a function of distance (Au-SMe), the covalent bond distance is found to be 2.4 Å, and the actual bending energy of approximately 0.96 eV, as illustrated in Fig. S7 (for more detail see the binding energy simulations in the SI).

To obtain a detailed understanding of electronic properties, the Frontier orbital of studied molecules: highest occupied molecular orbitals (HOMO) and lowest unoccupied orbitals (LUMO), along with their energies, were investigated. From the symmetry of these orbitals, an orbital product rule (OPR)[18] suggests that the shorter molecules (**1** and **2**), and long ones (**3** and **4**), exhibit a DQI at the most stable rotation angle ($\theta = 0°$), between the two Cp rings. This interference switches to a CQI for **1** and **3** when the rotation angles change to $\theta > 50°$ and $> 10°$ for **1** and **3** respectively, as shown in Fig. S3–S6 and summarised in Table S1.

Fig. 2a below, shows the ferrocene-based molecules **1** and **2** connected to Au electrodes. Fig. 2b shows that these junctions exhibit similar transmission functions $T(E)$ with a DQI transmission dip close to the HOMO resonance. This result suggests no significant difference in the conductance value specifically at the DFT-predicted Fermi energy ($E_F - E_F^{DFT} = 0$ eV) whether electrons pass through the iron (Fe), atom that linked the two cyclopentadienyl rings (**1**), or only through the upper CP ring
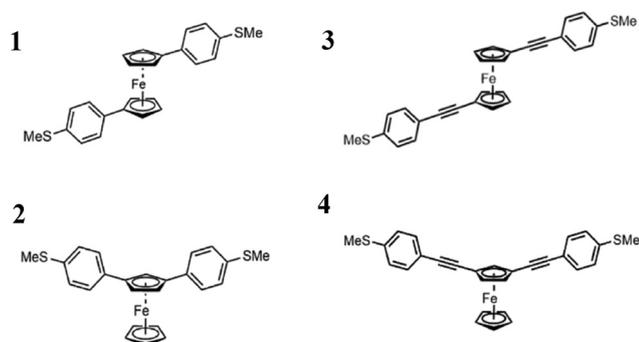

Fig. 1 Chemical structures of four different ferrocene-based derivatives in a different arrangement **1–4**. All derivatives end with the same terminal end group thioanisole (SMe).
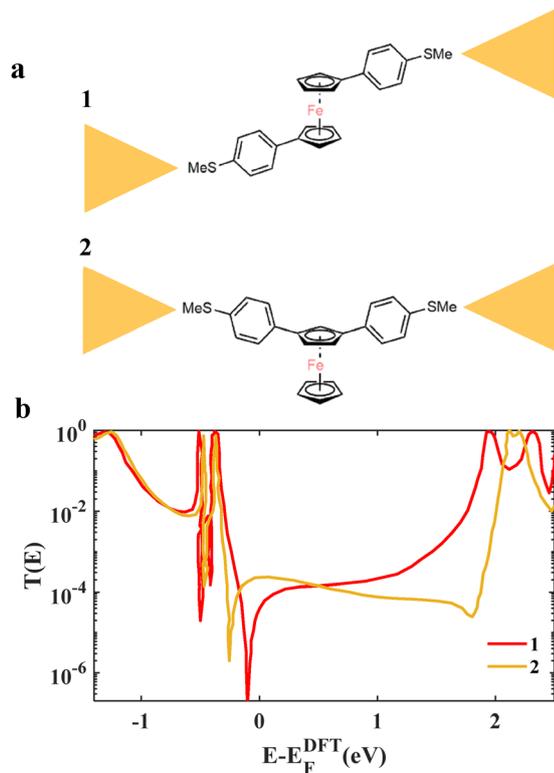
Fig. 2 (a) Schematic illustration of **1** and **2** ferrocene derivatives attached to two gold electrodes to form Au–ferrocene–Au junctions. (b) Zero bias transmission coefficients $T(E)$ against electron energy E for **1** and **2** of the short ferrocene derivatives at their most stable orientation. For **2** this corresponds to zero angle of rotation.

Fig. 3 (a) Illustration of the ferrocene unit under rotation. (b) Zero bias transmission coefficients $T(E)$ against electron energy E for **1** as a function of rotation of the ferrocene unit in different rotation degrees, $T(E)$ curves demonstrate the DQI move and vanish with rotation $0°$, $30°$, $40°$, $55°$, $90°$ and $120°$, in the HOMO–LUMO gap (Top panel). Bottom panel shows the Fano-shaped resonance appear in the HOMO–HOMO−1 gap for $90°$ and $120°$ (reproduced result, see ref. 1).

(**2**), as illustrated in Fig. 2b. Although both **1** and **2** manifest a DQI, however, this feature occurs slightly away from the Fermi level (E_F^{DFT}), about 0.1 eV and this is why it has limited influence on the conductance. This finding was reported in ref. 1.

In the same study,[1] they demonstrated how the rotation angle θ (Fig. 3a) can alleviate the DQI. Fig. 3b shows the DQI dip is at a lower energy when the rotation angle θ is zero (red curve), by increasing rotation angle the dip moves towards a higher energy (grey, green and purple curves), then it vanishes in the HOMO–LUMO gap at larger angles (*i.e.*, $\theta = 90°$ and $120°$, blue and orange curves respectively. The lower panel of Fig. 3b shows that the transmission function is a smooth function of energy within the HOMO–LUMO gap for $\theta = 90°$ and $120°$, which is a characteristic of CQI within the gap. On the other hand, both rotation angles produce a DQI feature at lower energy (in the HOMO−1 to HOMO gap), at roughly $E_F - E_F^{DFT} = -0.5$ eV, (shaded area). Therefore, rotating the Cp rings modifies interference and creates an extra DQI feature outside the HOMO–LUMO gap, while the DQI is alleviated inside the gap. It should be noticed that the anti-resonance within the H–L gap disappears completely at $\theta = 60°$ for the short ferrocene (**1**). These results agree-well with the OPR predictions (DQIs when $\theta < 60°$ and CQIs $\theta \geq 60°$), that shown in Fig S3 and Table S1.

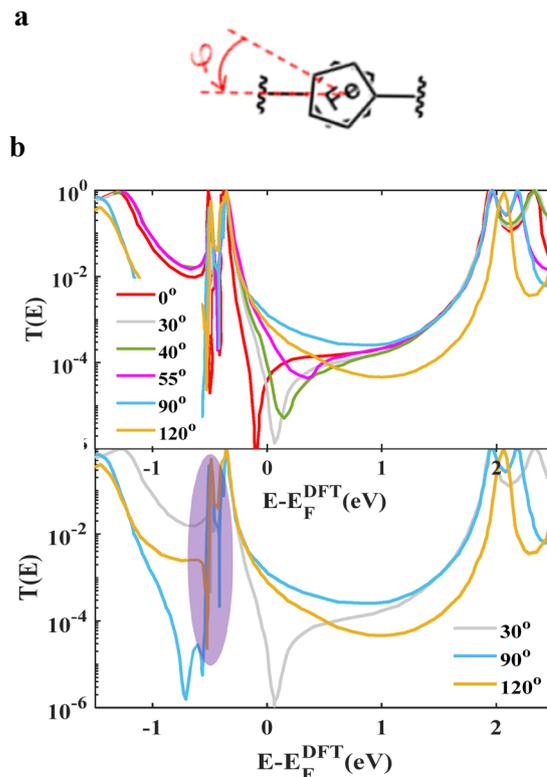We now investigate how this dependence on the rotation angle changes when the molecular length is increased to

include two extra triple bonds (–C≡C–), which increases the molecule length by ∼5 Å. The resulting ferrocenes **3** and **4** are shown in the right panel of Fig. 1. Again, we attached both ferrocenes **3** and **4** to gold electrodes as illustrated in Fig. 4a, and then calculated their transmission functions. Fig. 4b, shows that the transmission function for derivative **3** is much lower than that for **4** and for a wide range of energy >2 eV and the actual difference is approximately two orders of magnitude. Furthermore, the DQI dip feature is moved towards a higher energy (relative to the DQI-predicted Fermi energy), compared to the shorter derivative (**1**), as shown in the red curve of Fig. 2b. Similarly, the longer derivative **4** exhibits a dip, which is much closer to Fermi level $E_F - E_F^{DFT} = 0$ eV. Moreover, derivative **4** again presents a DQI feature within the HOMO−1 to HOMO gap, at roughly $E_F - E_F^{DFT} = -0.2$ eV, (shaded area) (Fig. 5).

The rotation simulations were repeated for the long ferrocene derivative (**3**), and again the DQI feature in the H–L gap disappears at specific rotation angle. Remarkably, this critical angle at which DQI switches to CQI is reduced to $\theta = 20°$, compared to $60°$ for the shorter molecule. Remarkably, the critical angle (θ) at which destructive quantum interference (DQI) transitions to constructive quantum interference (CQI) decreases significantly to $20°$ in the longer molecule, compared to $60°$ in its shorter counterpart. This substantial reduction
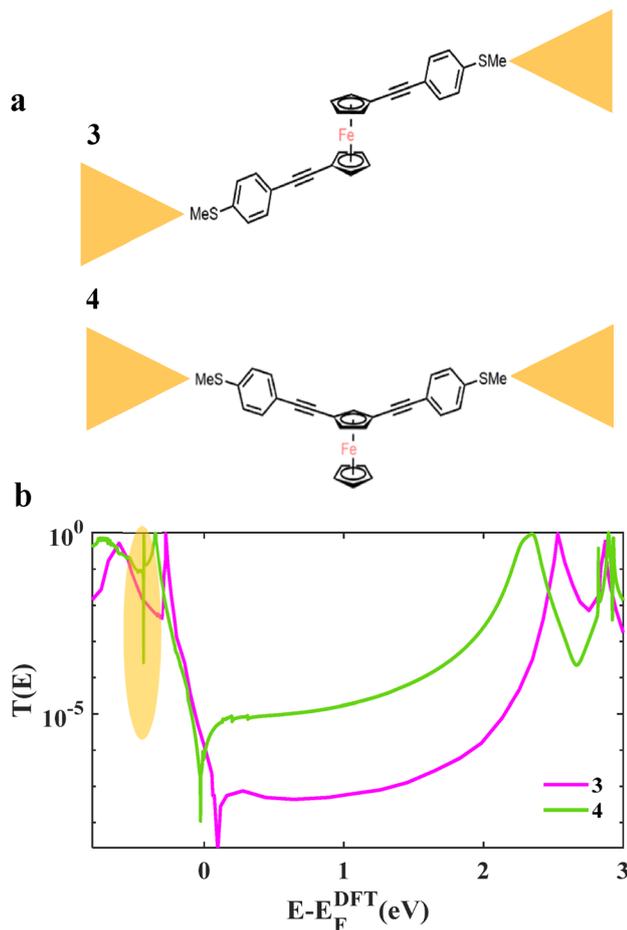
Fig. 4 (a) Schematic illustration of **3** and **4** ferrocene derivatives attached to two gold electrodes to form Au–ferrocene–Au junctions. (b) Transmission coefficients $T(E)$ against electron energy E for **3** and **4** of the longer ferrocene derivatives.

Fig. 5 (a) Illustration of the ferrocene unit rotation. (b) Zero bias transmission coefficients $T(E)$ against electron energy E for **3** as a function of rotation of the ferrocene unit in different rotation degrees, $T(E)$ curves demonstrate the DQI move and vanish with rotation 0°, 10°, and 20°, in the HOMO–LUMO gap. It also shows the Fano-shaped resonance appear in the HOMO–HOMO−1 gap for 20°.

highlights the pronounced sensitivity of quantum interference effects to molecular length. These DFT results are also reproduced by a simple tight binding model (TBM), and showed similar trend as shown in Fig. S9 and S11 of the SI.

To understand why longer molecules, enable transitions between DQI and CQI to occur at smaller rotation angles, it is useful to recall that QI effects can be regarded as arising from quantum interference between contributions from different molecular orbitals, as described in ref. 18. For example, an orbital product rule states that if the HOMO and LUMO have the same symmetry, then DQI occurs somewhere within the HOMO–LUMO gap, whereas if they have opposite symmetries, then CQI occurs. As discussed in ref. 18, this is only a qualitative guide. More generally, contributions from levels such as the HOMO−1, LUMO+1 and others should be included and the effect of their interferences depends on the amplitudes of the orbitals on the terminal groups of the molecule.

The symmetries and amplitudes of such levels are particularly sensitive to external perturbations when levels are almost degenerate. This can happen when continuous changes in some structural parameter, such as a rotation angle cause
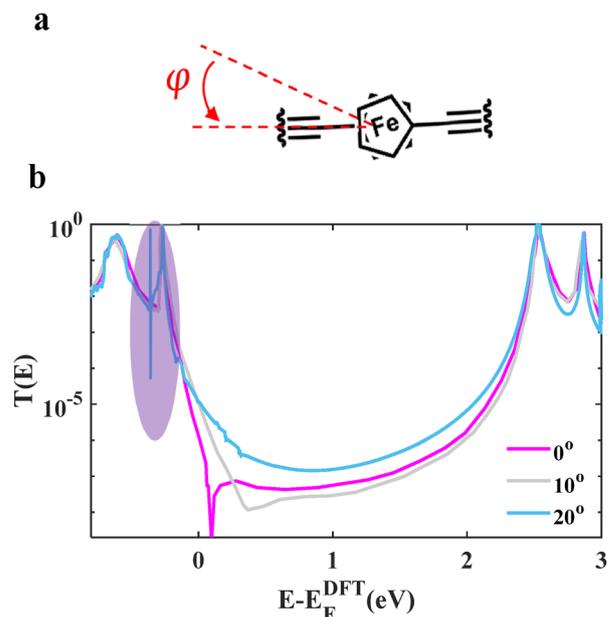
energy levels to cross or almost cross. Furthermore, typical level spacings tend to decrease as the size of a conjugated molecule is increased, the change in the structural parameter needed to shift energy levels by typical level spacings and cause such a crossing is smaller for larger molecules. This means that the change in the structural parameter needed to cause levels to cross and to experience changes in quantum interference is smaller for larger molecules.

The tendency for level crossing to occur at smaller rotational angles for the longer ferrocene 3 is demonstrated by the Fig. 7, which show that the HOMO−1 (H−1) crosses the HOMO (H) of the larger molecule 3 at a rotation angle of approximately 10°, compared with approximately 28° for the shorter molecule 1.

The Seebeck coefficient (S) is a fundamental parameter in molecular junctions, serving as a key indicator of their thermoelectric performance. It quantifies the magnitude and sign of the thermally induced voltage, providing critical insights into
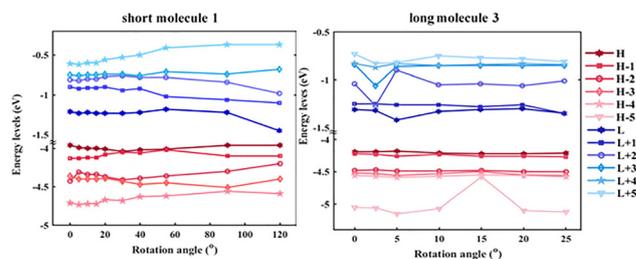

Fig. 6 Frontier molecular orbital energies *versus* rotation angle for molecules **1** and **3**.
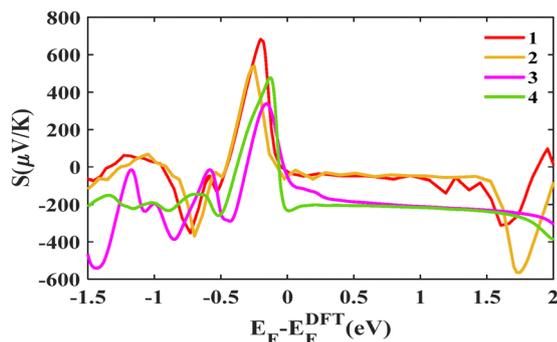
Fig. 7 Seebeck coefficients S as a function of the energy of molecules **1**–**4**. Shorter molecules (**1** and **2**), exhibit approximately zero S, whereas the long ones (**3** and **4**), show a high S around DFT-predicted Fermi energy. (Note S is calculated at $\theta = 0°$ for all molecules).

two essential aspects: (i) the junction's potential for energy harvesting applications, and (ii) the relative alignment between the electrode Fermi level and the molecular frontier orbitals (HOMO and LUMO). This alignment directly influences charge transport mechanisms, making S a vital metric for designing efficient molecular-scale thermoelectric devices. We also investigated the Seebeck coefficients of molecules **1** to **4**. Fig. 6 shows how extending the molecular length leads to a significant enhancement in value of the Seebeck coefficient around DFT-predicted Fermi energy. As shown by the purple and green curves (**3** and **4**), predicted enhancement is more than 250 μV K^{-1} around the DFT-predicted Fermi level. Transmission curve calculations above indicate a shift of the electrode Fermi level towards the HOMO as shown in Fig. 2b and 4b. This S enhancement is explained by the higher slope in the transmission function near the molecular resonance (HOMO/LUMO) region, as S is determined from Mott's formula:

$$S \approx -\frac{\pi^2 k_B^2 T}{3|e|}\left(\frac{d\ln(T(E_F))}{dE_F}\right)$$

4. Conclusions

In summary, we have studied the electrical conductance ferrocene-based molecular wires involving a Fe bridging atom between two cyclopentadienyl (CP) rings. For molecules **1** and **3**, whose rotation angle θ can be varied by changing the spacing between the electrodes, we find a that the length of the linkers plays a significant role in the angle-dependence of their electrical conductance. In particular DQI within the HOMO–LUMO gap is alleviated at entirely different rotation angle ($\theta > 20°$, compared to $> 60°$ for the shorter molecule). This shows that interference patterns within the ferrocene core are not simply a property of the core alone, but are a holistic property of the molecule as a whole.

We also found that the Seebeck coefficients of the longer molecules **3** and **4** reaches 250 μV K^{-1} around the DFT-predicted Fermi level, which is significantly higher that the Seebeck coefficients of the shorter molecules (**1** and **2**). These

finding open the way to designing new nanotechnology devices with potential practical applications.

Author contributions

A. K. I originally conceived the concept; calculations were carried out by K. A. A. A. A and A. A. All authors have given approval to the final version of the manuscript. All authors provided essential contributions to interpreting the data reported in this manuscript. A. K. I coordinated the writing of the manuscript with input from K. A. and A. A.

Conflicts of interest

There are no conflicts to declare.

Data availability

In this work, we use the following codes. 1-Siesta code used to predict the Hamiltonian of each system used in this study, which is located in **https://gitlab.com/siesta-project/siesta/-/releases**. 2-GOLLUM software is used to find the website's transmission coefficient. **https://www.gollumcode.com/**. 3-Conductance, Seebeck, and other parameters are calculated using the GOLLUM code **https://www.gollumcode.com/**.

Supplementary information: SI provides the electronic structure and thermoelectric properties of the studied molecules. See DOI: **https://doi.org/10.1039/d5qm00487j**.

References

1 M. Camarasa-Gómez, D. Hernangómez-Pérez, M. S. Inkpen, G. Lovat, E. D. Fung, X. Roy, L. Venkataraman and F. Evers, Mechanically Tunable Quantum Interference in Ferrocene-Based Single-Molecule Junctions, *Nano Lett.*, 2020, **20**(9), 6381–6386.

2 D. Astruc, Why is Ferrocene so Exceptional?, *Eur. J. Inorg. Chem.*, 2017, (1), 6–29.

3 L. A. Wilkinson, T. L. Bennett, I. M. Grace, J. Hamill, X. Wang, S. Au-Yong, A. Ismael, S. P. Jarvis, S. Hou and T. Albrecht, Assembly, structure and thermoelectric properties of 1, 1′-dialkynylferrocene 'hinges', *Chem. Sci.*, 2022, **13**(28), 8380–8387.

4 L. V. Snegur, Modern Trends in Bio-Organometallic Ferrocene Chemistry, *Inorganics*, 2022, **10**(12), 226.

5 T. L. Bennett, M. Alshammari, S. Au-Yong, A. Almutlg, X. Wang, L. A. Wilkinson, T. Albrecht, S. P. Jarvis, L. F. Cohen and A. Ismael, Multi-component self-assembled molecular-electronic films: towards new high-performance thermoelectric systems, *Chem. Sci.*, 2022, **13**(18), 5176–5185.

6 D. R. van Staveren and N. Metzler-Nolte, Bioorganometallic Chemistry of Ferrocene, *Chem. Rev.*, 2004, **104**(12), 5931–5986.

7 D. Astruc, From sandwich complexes to dendrimers: journey toward applications to sensing, molecular electronics, materials science, and biomedicine, *Chem. Commun.*, 2023, **59**(48), 7321–7345.

8 F. A. Larik, A. Saeed, T. A. Fattah, U. Muqadar and P. A. Channar, Recent advances in the synthesis, biological activities and various applications of ferrocene derivatives, *Appl. Organomet. Chem.*, 2017, **31**(8), e3664.

9 H. Werner, At Least 60 Years of Ferrocene: The Discovery and Rediscovery of the Sandwich Complexes, *Angew. Chem., Int. Ed.*, 2012, **51**(25), 6052–6058.

10 U. Siemeling, Singlet Carbenes Derived from Ferrocene and Closely Related Sandwich Complexes, *Eur. J. Inorg. Chem.*, 2012, (22), 3523–3536.

11 A. A. Al-Jobory and M. D. Noori, Thermoelectric properties of metallocene derivative single-molecule junctions, *J. Electron. Mater.*, 2020, **49**(9), 5455–5459.

12 C. Jia, I. M. Grace, P. Wang, A. Almeshal, Z. Huang, Y. Wang, P. Chen, L. Wang, J. Zhou, Z. Feng, Z. Zhao, Y. Huang, C. J. Lambert and X. Duan, Redox Control of Charge Transport in Vertical Ferrocene Molecular Tunnel Junctions, *Chem*, 2020, **6**(5), 1172–1182.

13 J. Ye, A. Al-Jobory, Q.-C. Zhang, W. Cao, A. Alshehab, K. Qu, T. Alotaibi, H. Chen, J. Liu and A. K. Ismael, Highly insulating alkane rings with destructive σ-interference, *Sci. China: Chem.*, 2022, **65**(9), 1822–1828.

14 A. A. Al-Jobory and A. K. Ismael, Controlling quantum interference in tetraphenyl-aza-BODIPYs, *Curr. Appl. Phys.*, 2023, **54**, 1–4.

15 B. Alanazi, A. Alajmi, A. Aljobory, C. Lambert and A. Ismael, Tuning quantum interference through molecular junctions formed from cross-linked OPE-3 dimers, *J. Mater. Chem. C*, 2024, **12**(19), 6905–6910.

16 F. Chen, Q.-M. Liang, L.-X. Lin, Q.-C. Zhang and Y. Yang, Recent progress in tuning charge transport in single-molecule junctions by substituents, *J. Mater. Chem. C*, 2023, **11**(42), 14515–14526.

17 X. Wang, A. Ismael, S. Ning, H. Althobaiti, A. Al-Jobory, J. Girovsky, H. P. Astier, L. J. O'Driscoll, M. R. Bryce and C. J. Lambert, Electrostatic Fermi level tuning in large-scale self-assembled monolayers of oligo (phenylene–ethynylene) derivatives, *Nanoscale Horiz.*, 2022, **7**(10), 1201–1209.

18 C. J. Lambert and S. X. Liu, A magic ratio rule for beginners: a chemist's guide to quantum interference in molecules, *Chem. – Eur. J.*, 2018, **24**(17), 4193–4201.

19 G. C. Solomon, J. P. Bergfield, C. A. Stafford and M. A. Ratner, When "small" terms matter: Coupled interference features in the transport properties of cross-conjugated molecules, *Beilstein J. Nanotechnol.*, 2011, **2**(1), 862–871.

20 M. Naher, *Structure–Property Relationships in Molecular Electronics*. 2021.

21 A. Ismael, X. Wang, A. Al-Jobory, S. Ning, T. Alotaibi, B. Alanazi, H. Althobaiti, J. Wang, N. Wei and C. J. Ford, Tuning the electrical conductance of oligo (phenylene-ethynylene) derivatives-PbS quantum-dot bilayers, *J. Mater. Chem. C*, 2024, **12**(35), 14004–14012.

22 X. Zhao, G. Kastlunger and R. Stadler, Quantum interference in coherent tunneling through branched molecular junctions containing ferrocene centers, *Phys. Rev. B*, 2017, **96**(8), 085421.

23 A. Alshehab and A. K. Ismael, Impact of the terminal end-group on the electrical conductance in alkane linear chains, *RSC Adv.*, 2023, **13**(9), 5869–5873.

24 X. Wang, A. Alajmi, Z. Wei, M. Alzanbaqi, N. Wei, C. Lambert and A. Ismael, Enhancing the Pressure-Sensitive Electrical Conductance of Self-Assembled Monolayers, *ACS Appl. Mater. Interfaces*, 2024, **16**(48), 66290–66300.

25 W. Lee, L. Li, M. Camarasa-Gómez, D. Hernangómez-Pérez, X. Roy, F. Evers, M. S. Inkpen and L. Venkataraman, Photo-oxidation driven formation of Fe-Au linked ferrocene-based single-molecule junctions, *Nat. Commun.*, 2024, **15**(1), 1439.

26 B. Pabi, J. Šebesta, R. Korytár, O. Tal and A. N. Pal, Structural Regulation of Mechanical Gating in Molecular Junctions, *Nano Lett.*, 2023, **23**(9), 3775–3780.

27 B. Lawson, P. Zahl, M. S. Hybertsen and M. Kamenetska, Formation and Evolution of Metallocene Single-Molecule Circuits with Direct Gold-π Links, *J. Am. Chem. Soc.*, 2022, **144**(14), 6504–6515.

28 H. Jeong, D. Kim, G. Wang, S. Park, H. Lee, K. Cho, W. T. Hwang, M. H. Yoon, Y. H. Jang and H. Song, Redox-induced asymmetric electrical characteristics of ferrocene-alkanethiolate molecular devices on rigid and flexible substrates, *Adv. Funct. Mater.*, 2014, **24**(17), 2472–2480.

29 A. K. Ismael and C. J. Lambert, Molecular-scale thermoelectricity: a worst-case scenario, *Nanoscale Horiz.*, 2020, **5**(7), 1073–1080.

30 M. Alshammari, A. A. Al-Jobory, T. Alotaibi, C. J. Lambert and A. Ismael, Orientational control of molecular scale thermoelectricity, *Nanoscale Adv.*, 2022, **4**(21), 4635–4638.

31 G. Nemnes and A. Nicolaev, Transport in ferrocene single molecules for terahertz applications, *Phys. Chem. Chem. Phys.*, 2014, **16**(34), 18478–18482.

32 A. R. Garrigues, L. Yuan, L. Wang, S. Singh, E. Del Barco and C. A. Nijhuis, Temperature dependent charge transport across tunnel junctions of single-molecules and self-assembled monolayers: a comparative study, *Dalton Trans.*, 2016, **45**(43), 17153–17159.

33 Q. Lu, C. Yao, X. Wang and F. Wang, Enhancing Molecular Conductance of Oligo(p-phenylene ethynylene)s by Incorporating Ferrocene into Their Backbones, *J. Phys. Chem. C*, 2012, **116**(33), 17853–17861.

34 Y.-Y. Sun, Z.-L. Peng, R. Hou, J.-H. Liang, J.-F. Zheng, X.-Y. Zhou, X.-S. Zhou, S. Jin, Z.-J. Niu and B.-W. Mao, Enhancing electron transport in molecular wires by insertion of a ferrocene center, *Phys. Chem. Chem. Phys.*, 2014, **16**(6), 2260–2267.

35 L. Zhang, Y. Zhao, W. Kong, H. Zhang, L. Zang, M. Zhao, J. Zhang, R. M. Kong, E. S. Zhang and F. Qu, Functional Metallocenes as Cofactors Promote the Catalytic Performance of Mimetic Enzymes, *Small*, 2025, **21**(1), 2405851.

36 H. Takashima, Y. Inagaki, H. Momma, E. Kwon, K. Yamaguchi and W. Setaka, Ferrocene-diyl bridged macrocages: steric effects of the cage on the redox properties of ferrocene moiety, *Organometallics*, 2018, **37**(9), 1501–1506.

37 H. Jeong, Y. Jang, D. Kim, W.-T. Hwang, J.-W. Kim and T. Lee, An in-depth study of redox-induced conformational changes in charge transport characteristics of a ferrocene-alkanethiolate molecular electronic junction: Temperature-dependent transition voltage spectroscopy analysis, *J. Phys. Chem. C*, 2016, **120**(6), 3564–3572.

38 M. Alshammari, S. Alhassan, K. Alshammari, T. Alotaibi, A. H. Alshammari, S. Alotibi, T. A. M. Taha and A. Ismael, Hydrogen catalytic performance of hybrid $Fe_3O_4/FeS_2/g$-C_3N_4 nanocomposite structures, *Diamond Relat. Mater.*, 2023, **138**, 110214.

39 Y. Cai, Y. Gao, Q. Luo, M. Li, J. Zhang, H. Tian and W. H. Zhu, Ferrocene-grafted photochromic triads based on a sterically hindered ethene bridge: Redox-switchable fluorescence and gated photochromism, *Adv. Opt. Mater.*, 2016, **4**(9), 1410–1416.

40 T. A. M. Taha, S. S. Alanazi, K. S. El-Nasser, A. H. Alshammari and A. Ismael, Structure–property relationships in $PVDF/SrTiO_3/CNT$ nanocomposites for optoelectronic and solar cell applications, *Polymers*, 2024, **16**(6), 736.

41 A. K. Ismael, 20-State Molecular Switch in a Li@ C60 Complex, *ACS Omega*, 2023, **8**(22), 19767–19771.

42 Y. Yokota, Y. Mino, Y. Kanai, T. Utsunomiya, A. Imanishi and K.-I. Fukui, Electronic-state changes of ferrocene-terminated self-assembled monolayers induced by molecularly thin ionic liquid layers: A combined atomic force microscopy, X-ray photoelectron spectroscopy, and ultraviolet photoelectron spectroscopy study, *J. Phys. Chem. C*, 2015, **119**(32), 18467–18480.

43 J.-L. Hou, W. Luo, Y. Guo, P. Zhang, S. Yang, Q.-Y. Zhu and J. Dai, Titanium oxo cluster with six peripheral ferrocene units and its photocurrent response properties for saccharides, *Inorg. Chem.*, 2017, **56**(11), 6451–6458.

44 S. Yuan, S. Wang, Z. Kong, Z. Xu, L. Yang, D. Wang, Q. Ling and Y. Wang, Theoretical studies of the spin-dependent electronic transport properties in ethynyl-terminated ferrocene molecular junctions, *Micromachines*, 2018, **9**(3), 95.

45 T. P. Gryaznova, S. A. Katsyuba, V. A. Milyukov and O. G. Sinyashin, DFT study of substitution effect on the geometry, IR spectra, spin state and energetic stability of the ferrocenes and their pentaphospholyl analogues, *J. Organomet. Chem.*, 2010, **695**(24), 2586–2595.

46 A. Ismael, A. Al-Jobory, X. Wang, A. Alshehab, A. Almutlg, M. Alshammari, I. Grace, T. L. Benett, L. A. Wilkinson and B. J. Robinson, Molecular-scale thermoelectricity: as simple as 'ABC', *Nanoscale Adv.*, 2020, **2**(11), 5329–5334.

47 A. K. Ismael, T. A. Mohaymen Taha and A. Al-Jobory, Three distinct conductance states in polycyclic aromatic hydrocarbon derivatives, *R. Soc. Open Sci.*, 2024, **11**(6), 231734.

48 J. M. Soler, E. Artacho, J. D. Gale, A. García, J. Junquera, P. Ordejón and D. J. Sánchez-Portal, The SIESTA method for ab initio order-N materials simulation, *J. Phys.: Condens. Matter*, 2002, **14**(11), 2745.

49 A. K. Ismael, A. Al-Jobory, I. Grace and C. J. Lambert, Discriminating single-molecule sensing by crown-ether-based molecular junctions, *J. Chem. Phys.*, 2017, **146**, 6.

50 A. K. Ismael, I. Grace and C. J. Lambert, Increasing the thermopower of crown-ether-bridged anthraquinones, *Nanoscale*, 2015, **7**(41), 17338–17342.